Miscible density-driven flows in heterogeneous porous media: Influences of correlation length and distribution of permeability

Qian Li, Weihua Cai,* Feng-Chen Li, and Bingxi Li
School of Energy Science and Engineering, Harbin Institute of Technology, Harbin, China

Ching-Yao Chen†
Department of Mechanical Engineering, National Chiao Tung University, Hsinchu, Taiwan

(Received 26 July 2018; published 4 January 2019)

A random process and highly accurate pseudospectral method associated with compact finite differences are incorporated to evaluate effects of permeability heterogeneity to gravity-driven miscible porous media flows. Flows in heterogeneous permeability fields, based on multiple sets of random realizations with identical statistical characteristics, are simulated to elucidate the global trend of mean quantities and local variations. The presence of heterogeneity provokes more prominent fingering competition and greater variation of fingers' widths, hence the mean values of interested quantitative measures, i.e., breakthrough time, amount of fluid volumes transported, and normalized mixing effectiveness, are generally reduced. Resonant effects, whose influences on the flow fields are the most significant, are verified to occur in an intermediate correlation length, in which the widths of fingers are slightly less than the correspondent correlation length. Nevertheless, under the resonant conditions these measures are the most widely scattered between different random realizations associated with the same control parameters. The widest scatterings are mainly because of the enhancing sensitivity of flow path selections under such resonant conditions, especially in a few realizations whose high or low permeability regions align along with or transverse to the main flow direction. The significant scatterings of these quantitative measures, which had drawn little attention previously, suggest more cautious treatments for practical implementations in the regime of resonant effects.

DOI: 10.1103/PhysRevFluids.4.014502

I. INTRODUCTION

Viscous fingering instability, or the Saffman-Taylor instability [1], in a porous medium or Hele-Shaw cell has long been an ongoing subject under thorough study for many decades. Comprehensive reviews regarding the fundamental theory and popular applications are provided by Refs. [2,3]. Because of the concerns about global warming, a recent and important application of this classic problem related to the subsurface storage of carbon dioxide (CO_2) has also drawn much attention. A practical option of CO_2 storage is injecting CO_2 in a supercritical state, i.e., under a condition of high temperature and enormous pressure, into porous rocks in the deep subsurface, such as depleted oil and gas reservoirs [4–6]. To achieve stable long-term and large-scale storage, one of the efficient ways is to dissolve CO_2 into the surrounding brine. In saline aquifers, the supercritical CO_2 is less dense (200–700 kg/m^3) than the ambient brine (900–1200 kg/m^3), so that the injected

*caiwh@hit.edu.cn
†chingyao@mail.nctu.edu.tw

supercritical CO_2 will float on the top of saline aquifers to reside beneath the cap rocks. A tank of supercritical CO_2 will be formed above the brine water with a stable interface between them. It is known that CO_2 is partially miscible to the brine water, typically 3% in weight under the subsurface condition [7]. Nevertheless, the CO_2-brine mixture is generally about 14 kg/m^3 heavier than pure brine [8], so that the miscible system becomes unstable to trigger natural convection. The dissolution-driven convection greatly enhances the process of dissolution of CO_2 into the brine. This interesting phenomenon had been experimentally studied in a Hele-Shaw cell [9–14], which is commonly used to represent a homogeneous porous condition. The dissolution-driven convection was substantiated when high-pressure CO_2 (6 bar) was injected in a Hele-Shaw cell to dissolve into the top layer of water [9,10]. Alternatively, lighter water placed over heavier propylene glycol, whose mixture is heavier than both, also appears similar to dissolution-driven convection in a Hele-Shaw cell [11,12]. In addition, potassium permanganate ($KMnO_4$) in water was also used as an analog for CO_2 in brine to successfully obtain dissolution-driven convection with apparent fingering patterns [14]. On the other hand, numerical simulations dealing with this dissolution-driven fingering patterns for CO_2 storage based on the Hele-Shaw equations, or the homogeneous Darcy's law, had also been presented [15,16]. More practically, Szulczewski *et al.* [17] conducted simulations, by assuming a top layer of CO_2 source, to investigate fingering patterns in structural and stratigraphic layer. Fully three-dimensional simulations with high resolution were also preformed [18].

All of the aforementioned works were studied in homogeneous and isotropic porous media or Hele-Shaw cells. As for anisotropic porous media, there are relative fewer studies focusing on dissolution-driven fingering problems. Recent results revealed that the amount of CO_2 dissolved in anisotropic sedimentary rocks is much larger than in isotropic rocks [19–21]. On the other hand, intensive research had be carried out to understand the effects of heterogeneity on conventional viscous fingering by displacements, since the pioneering experiments reported several decades ago [22]. Subsequently, analytical and numerical studies were well presented, e.g., by highly accurate pseudospectral simulations [23–31] or a particle-tracking method [32]. With strong variation of permeability, fingering patterns are dictated by the permeability distribution. When the characteristic length scale of permeability distribution is close to the fingering scale, a resonant amplification of instability was proposed [24,33,34]. In horizontal layered heterogeneous media, several distinct regimes of the flow displacement were also identified [35].

In practical applications, the CO_2 storage sites are naturally heterogeneous. The heterogeneity is expected to play important roles for the fingering patterns as well as quantitative measures of interest, such as the volumes of CO_2 transported downward, and mixed with the brines. In the present study, we focus on the density-driven convection of a binary system, i.e., heavier CO_2-brine mixture and pure brine, in heterogeneous porous media with different random distributions. In addition to the qualitative observations of fingering patterns, we emphasize both the global mean values and local variations of interested measures among the different random realizations with identical control parameters of statistical characters. It is noticed that even the global trend of some results had been reported before, which was mainly demonstrated in a single particular permeability distribution, but the local variations between different random realizations had not been discussed to the best of our knowledge. For better implementation to practical applications, it is equally important to reveal the local behaviors of all the distinct permeability distributions perturbed by different sets of random signals. To thoroughly investigate both the global and local behaviors, a classic random process is elaborated in detail and adopted to generate permeability fields with the desired statistical parameters, e.g., correlation length and variance, with multiple realizations of random signals. All heterogeneity conditions are simulated by eight realizations to elucidate their trends of a global statistic mean as well as local variation among them.

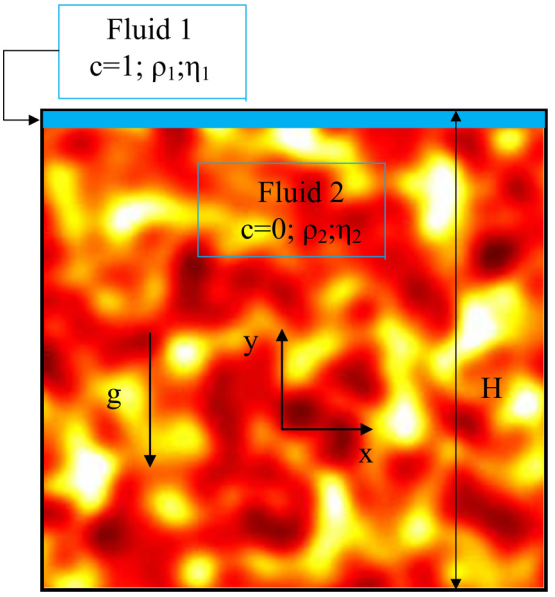

FIG. 1. Representative sketch of a square heterogeneous porous medium with dimension H, where a clearer (darker) area corresponds to a region of higher (lower) permeability. Fluid 1 occupied on the top layer is heavier and less viscous than the lower fluid 2, i.e., $\rho_1 > \rho_2$ and $\eta_1 < \eta_2$, so that the miscible interface is gravitationally unstable to produce complex fingering pattern.

II. PHYSICAL PROBLEM AND MATHEMATICAL MODELS

A. Governing equations

We numerically study a binary system containing two incompressible viscous fluids in a square two-dimensional heterogeneous porous medium with dimension H, in which the permeability distribution is $k(x, y)$, as shown in Fig. 1. The two fluids are miscible to each other, whose viscosities/densities are denoted as η_1/ρ_1 (fluid 1), and η_2/ρ_2 (fluid 2), respectively. Fluid 1 is assumed heavier and less viscous, i.e., $\rho_1 > \rho_2$ and $\eta_2 > \eta_1$. A thin layer of the fluid 1 reservoir is placed on top of the square domain, so that fluid 1 is continuously supplied within this region. Excluding the region of this top layer, the porous medium is initially fully occupied by fluid 2. A Cartesian coordinate system (x, y) is defined in such a way that its origin is located at the center of the square domain. Under the present condition, the fluid-fluid interface is gravitationally and viscously unstable. The system in such a two-dimensional heterogeneous porous medium is governed by the following set of Darcy's equations [23–28]:

$$\nabla \cdot \mathbf{u} = 0, \tag{1}$$

$$\nabla p = -\frac{\eta}{k}\mathbf{u} - \rho \mathbf{g}, \tag{2}$$

$$\frac{\partial c}{\partial t} + \mathbf{u} \cdot \nabla c = D\nabla^2 c. \tag{3}$$

Here $\mathbf{u}$, p, η, and ρ denote the velocity vector, the pressure, the viscosity, and the density of the binary system, respectively. $\mathbf{g}$ is the gravity vector pointing downward, i.e., the negative y direction. c represents fluid concentration, such that $c = 1$ and $c = 0$ for the less viscous fluid 1 and the more

viscous fluid 2, respectively. The constant D is the coefficient of diffusion. The correlations of viscosity and density with concentration are assumed to be related as

$$\eta(c) = \eta_1 e^{[R(1-c)]}, \quad R = \ln\left(\frac{\eta_2}{\eta_1}\right), \tag{4}$$

$$\rho(c) = \rho_2 + c\Delta\rho. \tag{5}$$

R is a control parameter of the viscosity contrast, and $\Delta\rho$ is the density difference between fluids: $\Delta\rho = \rho_1 - \rho_2$.

B. Permeability heterogeneity

In order to systematically evaluate the influences of permeability heterogeneity, the permeability field $k(x, y)$ is assumed as log-normal distributions associated with desired statistical characteristics, i.e., the correlation length l and the variance s [23–25,27–31]. In such a way, the permeability is expressed in terms of a characteristic permeability K and a Gaussian-like zero-mean function $f(x, y)$, $\overline{f(x, y)} = 0$, such that [24]

$$k(x, y) = K e^{s^2 f(x,y)}. \tag{6}$$

This expression gives a logarithmic mean permeability of $\overline{\log_e[k(x, y)]} = \log_e[K]$. Within this description, changes in the magnitude of the permeability are determined by the variance s. Note that, by considering the limit of vanishing variance, $s = 0$, one reproduces a homogeneous medium situation.

To prescribe the typical size of more or less permeable regions by the correlation length l, an algorithm originally proposed by Shinozuka and Jan [36] for digital simulation of a random process is employed to generate such a random Gaussian-like function, expressed as

$$f(\mathbf{x}) = \sqrt{2}\sum[B^2(\mathbf{x}, \omega_\mathbf{i})S_0(\omega_\mathbf{i})\Delta\omega]^{1/2}\cos(\acute{\omega_i}\cdot\mathbf{x} + \psi_i), \tag{7}$$

where $B(\mathbf{x}, \omega_\mathbf{i})$ and $S_0(\omega_\mathbf{i})$ are a two-dimensional modulating function and the target spectral density, respectively, and $\mathbf{x}$ is the dimensional vector. In the present study, a simple constant $B = 1$ is applied. To generate a Gaussian-like function, the target spectral density S_0 is taken as

$$S_0 = \frac{l_1 l_2}{2\pi\sigma^2}\, e^{[(l_1\omega_1)^2 + (l_2\omega_2)^2/2\sigma^2]}, \tag{8}$$

in which subscripts 1 and 2 specify variables in different dimensions, e.g., x and y, so that $l_1 = l_2 = l$ in the present case. σ is the variance of the spectral density and is taken as $\sigma = \sqrt{2\pi}$ here. To cover the entire spectral density, $\omega \in [-100, 100]$ is calculated in both dimensions. The set of independent random signals ψ_i involved in the permeability distribution is generated by Matlab, which is bounded between 0 and 2π. These random signals are also used to perturb ω_i, so that periodicity can be avoided. In such a way, the perturbed $\acute{\omega}_i$ is expressed as

$$\acute{\omega}_i = \omega_i + \delta\omega_i, \tag{9}$$

where $\delta\omega_i = \psi_i\Delta\omega$.

To statistically investigate the effects of permeability heterogeneity, eight permeability realizations, by applying different sets of random signals ψ, associated with identical statistical features, e.g., correlation length l and variance s, are simulated in the present study. For readers' easier reference, four representative dimensionless heterogeneous permeability distributions of $s = 0.6$ generated by the first set of random signals associated with various correlation lengths of $l = 0.08$, 0.2, 0.4, and 0.8, are demonstrated in Fig. 2 and referred to as the R1 permeability distribution hereinafter. It is noticed that the permeability is scaled by K, so that $\overline{\log_e[k(x, y)]} = 0$.

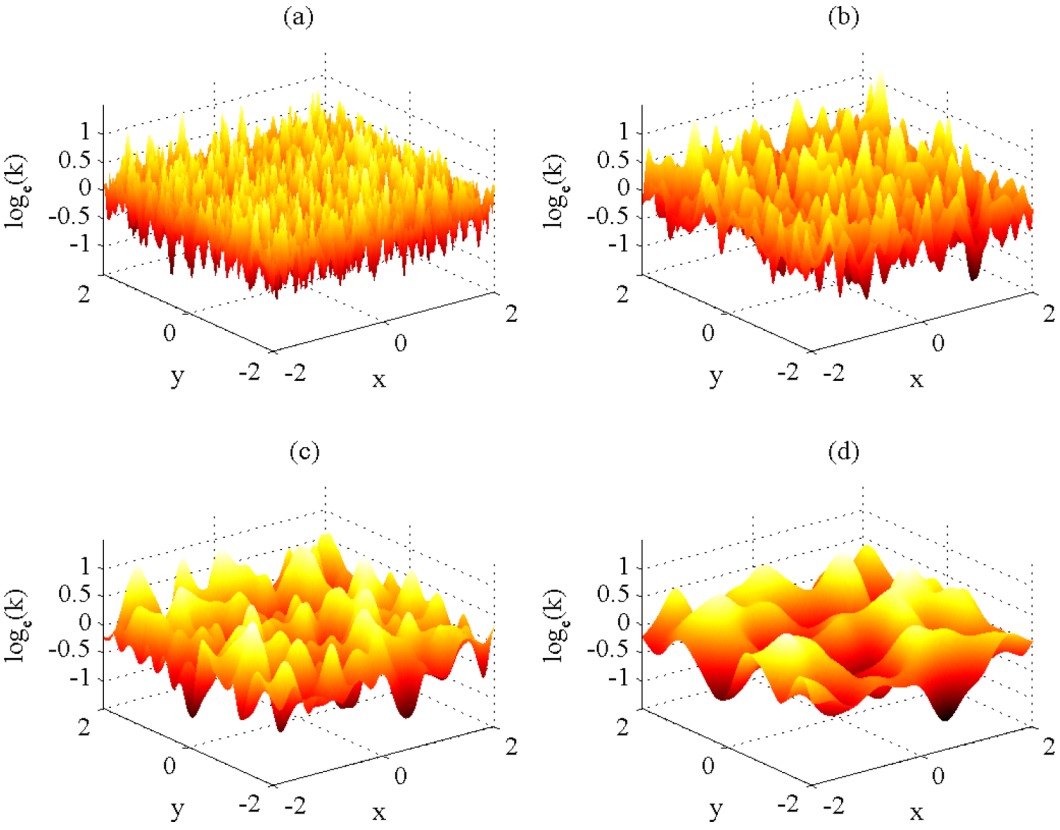

FIG. 2. Reference distributions of heterogeneous permeability fields generated by a representative set of random signals, denoted as the R1 realizations, for various correlation lengths of $l =$ (a) 0.08, (b) 0.2, (c) 0.4, and (d) 0.8. The fields follow the log-Gaussian distributions with vanishing logarithm means, i.e., $\overline{\log_e k(x, y)} = 0$.

C. Numerical methods

In order to render the governing equations and relevant variables dimensionless, $H/4$, η_1, $\Delta\rho$, and K are taken as the characteristic scales, such that the time, the velocity, and the pressure are scaled by $\eta_1 H/4\Delta\rho g K$, $\Delta\rho g K/\eta_1$, and $\Delta\rho g H/4$, respectively. Furthermore, to use the numerical scheme with high order of accuracy already employed in Refs. [25,27,28], the dimensionless governing equations are reformulated into the well-known streamfunction (ϕ)–vorticity (ω) system and yield

$$\frac{\partial \phi}{\partial y} = u, \quad \frac{\partial \phi}{\partial x} = -v, \tag{10}$$

$$\nabla^2 \phi = -\omega, \tag{11}$$

$$\frac{\partial c}{\partial t} + \mathbf{u} \cdot \nabla c = \frac{1}{\mathrm{Pe}} \nabla^2 c, \tag{12}$$

where

$$\omega = -R\left(u\frac{\partial c}{\partial y} - v\frac{\partial c}{\partial x}\right) - \frac{1}{k}\left(u\frac{\partial k}{\partial y} - v\frac{\partial k}{\partial x}\right) - \frac{k}{\eta}\frac{\partial c}{\partial x}.$$

In the context of the present problem, dimensionless controlling parameters such as the Péclet number Pe (relative measure of advection and diffusion effects), and the Atwood number A (normalized viscosity difference) are defined as

$$\mathrm{Pe} = \frac{\Delta\rho g H K}{\eta_1 D}, \quad \mathrm{A} = \frac{e^R - 1}{e^R + 1}.$$

Using the above settings, the simulations are performed in a square computational domain with a dimensionless length of 4. Simulations are terminated shortly before the most downward finger reaches close to the bottom boundary, denoted as the breakthrough time t_b. The boundary conditions are prescribed as follows:

$$x = \pm 2\text{: } \phi = 0, \quad \frac{\partial c}{\partial x} = 0, \tag{13}$$

$$y = \pm 2\text{: } \phi = 0, \quad \frac{\partial c}{\partial y} = 0. \tag{14}$$

As mentioned above, highly accurate numerical schemes are essential to reproduce extremely fine structures of induced fingers. To achieve this, spatial derivatives in the concentration equation are discretized by compact finite differences with a fourth and sixth order of accuracy for convective and diffusive terms, respectively, associated with third-order Runge-Kutta procedure for time integration. The Poisson equation of a streamfunction is solved by a pseudospectral method associated with discretization of a sixth-order compact finite difference in space. The simulations using similar schemes [25,27] were validated by comparing the growth rates in a homogeneous condition with the respective values obtained from linear stability theory. For a more detailed account of these numerical schemes, readers are referred to Ref. [37].

III. RESULTS AND DISCUSSION

The main theme of the present study is to evaluate the effects of heterogeneity on the miscible viscous fingering phenomena triggered by gravitation. In the following presentations, we focus on the situations of $\mathrm{A} = 0.76$ and $\mathrm{Pe} = 4000$, in which viscous fingering is vigorous even in a homogeneous condition, i.e., $s = 0$ or $l = 0$. The magnitude of permeability heterogeneity is fixed at $s = 0.6$ for all cases, such that the magnitudes of permeability vary between $e^{-1.5} < k(x, y) < e^{1.5}$ as the representative R1 series shown in Fig. 2.

A. Flow patterns: Representative series

Figure 3 shows the fingering patterns for the representative R1 series at the corresponding breakthrough time, when the heavier fluid reaches the bottom and is denoted as t_b, for various correlation lengths, e.g., the homogeneous case ($s = 0$ or $l = 0$) and $l = 0.08, 0.2, 0.4, 0.8, 2$. As reported in the early literatures applying similar methodology [24,25,28,29], which mainly investigated radially displacements, fingering patterns are immediately altered by the presence of permeability heterogeneity. For the cases whose correlation lengths is relatively shorter, e.g., $l = 0.08$ and 0.2, small disturbances by the permeability heterogeneity result in rough fingering interfaces with numerous fine structures. On the other hand, fingering interfaces appear smooth for the cases of longer correlation lengths of $l = 0.8$ and 2.

Two major qualitative effects of the permeability heterogeneity to the fingering pattern are reviewed: (1) prominent finger competition and (2) significant variation of widths of fully evolved fingers. Fingering competition, which refers to uneven growths of a few dominant fingers, is often observed in conventional viscous fingering instability. More prominent fingering competition in the cases associated with permeability heterogeneity, which may provide preferable paths of high permeability to enhance the growths of particular fingers, can be apparently identified by the concentration images shown in Fig. 3. For the homogeneous condition, several fingers evolve

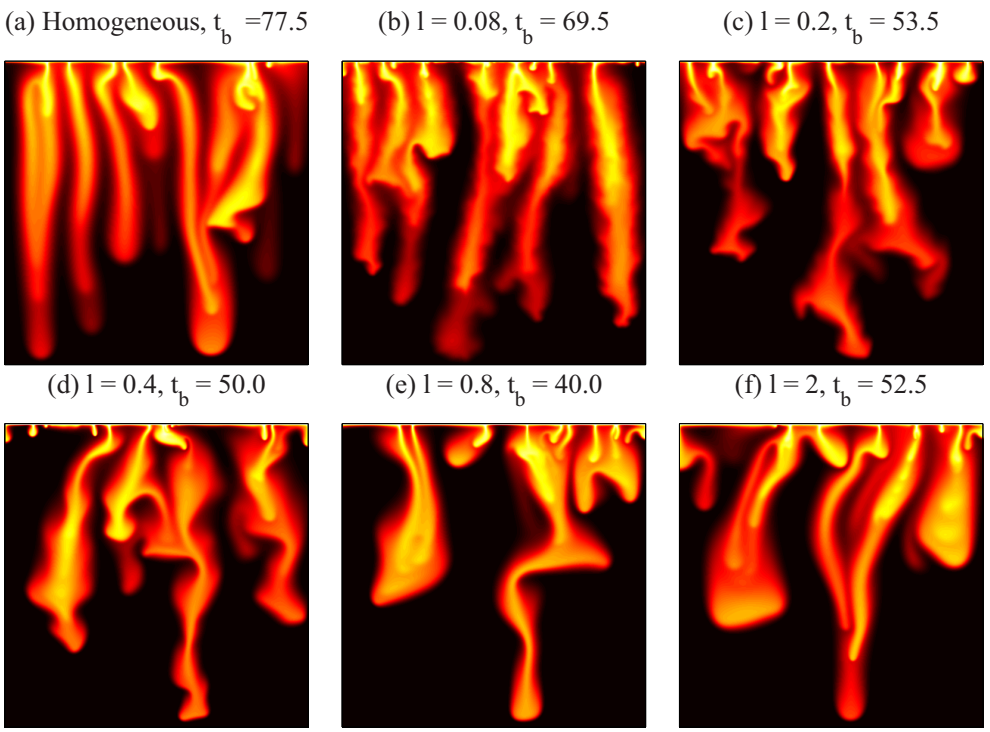

FIG. 3. Concentration images at the breakthrough time (t_b) in the R1 permeability realizations. (a) Homogeneous condition ($s = 0$), (b) $l = 0.08$, (c) $l = 0.2$, (d) $l = 0.4$, (e) $l = 0.8$, and (d) $l = 2$. Notice that the correspondent permeability fields for conditions of $l = 0.08$, 0.2, 0.4, and 0.8 are shown in Fig. 2. The fastest breakthrough occurs in the case of intermediate correlation length $l = 0.8$.

comparably; see, e.g., Fig. 3(a). Because these capably evolved fingers to accommodate more amount of heavier fluids, the breakthrough time is put off to occur at $t_b = 77.5$ in the homogeneous case. The prominence of fingering competition is enhanced in the heterogeneous conditions, in which fewer dominant fingers outgrow their counterparts to shorten the breakthrough time. The competition appears the most significant for the case of $l = 0.8$, which leads to the earliest breakthrough time at $t_b = 40$. Since the present fingering competition is mainly caused by the local permeability variation instead of the conventional viscous fingering mechanism, it was referred as to *channeling* effects [24,25,28–30]. In addition, under the presence of permeability heterogeneity, the width of a finger's body varies significantly at different sections, i.e., root, body, and tip, while most of the fingers in the homogeneous condition evolve more evenly with nearly uniformed widths along the entire fingers. This apparent variation of fingers' widths is resulted from significant transverse (x-directional) motion because of permeability heterogeneity. The transverse motion tends to widen the flow path, so that the finger body generally appears thicker. Greater variations of fingers' sizes are observed in the cases of longer correlation lengths, e.g., $l = 0.8$ and 2. It is noticed that the dominant width of the fully evolved finger was argued to be an important factor to trigger the so-called *resonant* effect, which often occurs in intermediate correlation lengths, e.g., $l = 0.8$ in the present series, to maximize the growth rate of fingered zone (equivalent to the length of the most downward finger in the present gravity-driven situation) [23] and trigger the earliest breakthrough time [24,30]. More discussion regarding these two major qualitative observations is presented below.

To elucidate the fingering competition in a temporal manner, the evolutions of concentration along the top cross section at $y = 1.97$ for the cases shown in Fig. 3 are plotted in Fig. 4. It

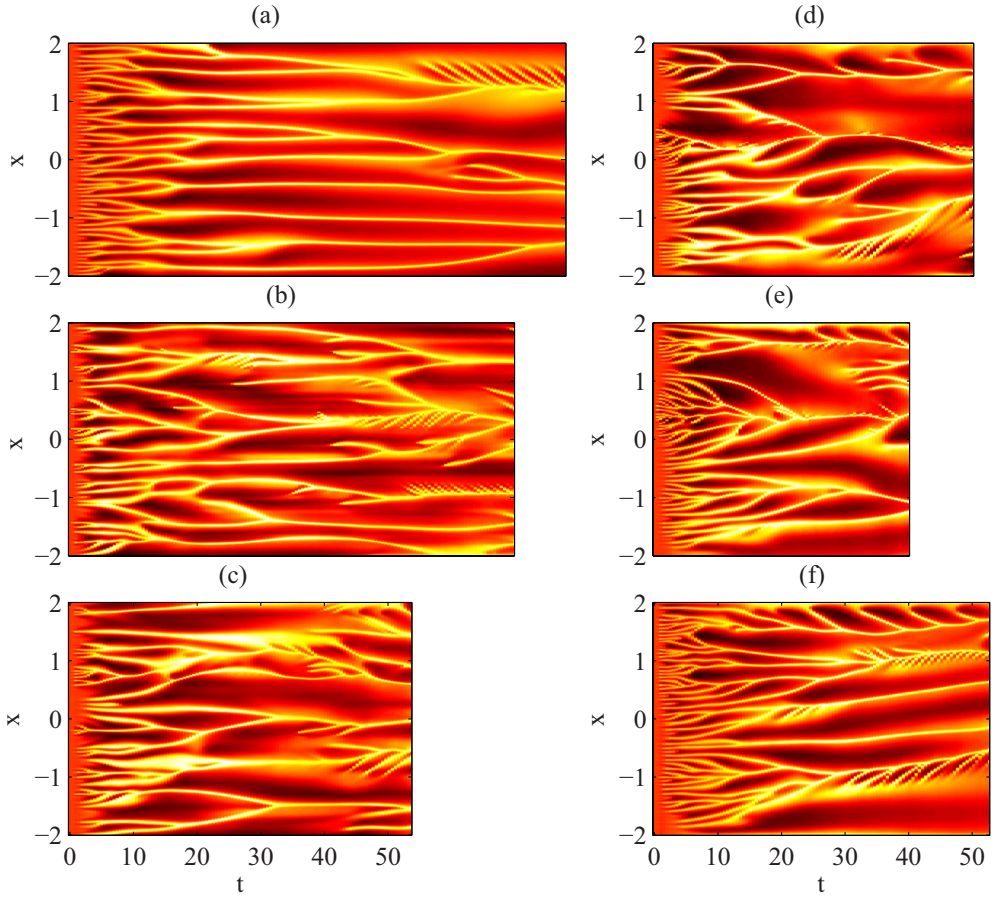

FIG. 4. Temporal concentration distribution measured along the top cross section at $y = 1.97$ through the entire simulated period, i.e., $t = 0 \sim t_b$, for the cases shown in Fig. 3. (a) Homogeneous, (b) $l = 0.08$, (c) $l = 0.2$, (d) $l = 0.4$, (e) $l = 0.8$, and (f) $l = 2$.

has been concluded that three major regimes can be identified in a homogeneous porous medium [20], such as flux growth, merging, and constant flux. All three regimes are reproduced in the present homogeneous simulation, as shown in Fig. 4(a). The regime of flux growth is manifested by generation of an increasing number of fine fingers at a very early time stage $0 < t < 5$. These numerous fine fingers proceed active merging at the middle time stage $5 < t < 20$ and finally form a few dominant fingers after $20 < t < t_b$. The nearly constant number of dominant fingers at this final stage indicates the flux flows downward to the porous medium do not vary significantly, so that is referred to as the constant flux regime. However, even the regime of flux growth can be clearly identified for all heterogeneous cases, and the merging regime is prolonged very significantly. The time period of constant flux regime, whose pattern appears as formation of a nearly fixed number of isolated fingers without interaction, is shortened for larger correlation length for cases $l \leqslant 0.8$. For the resonant case of $l = 0.8$, the merging behavior lasts through the entire period without the final regime of constant flux. The evolution of extremely active merging indicates a strong fingering selection process, i.e., fingering competition. Beyond this resonant value of correlation length, e.g., $l = 2$, the merging activity is weakened, and the regime of constant flux is slightly recovered.

To further characterize the fingering competition spatially, the average concentration profiles along the transverse (x) direction, denoted as c_a, for various correlation lengths at different times

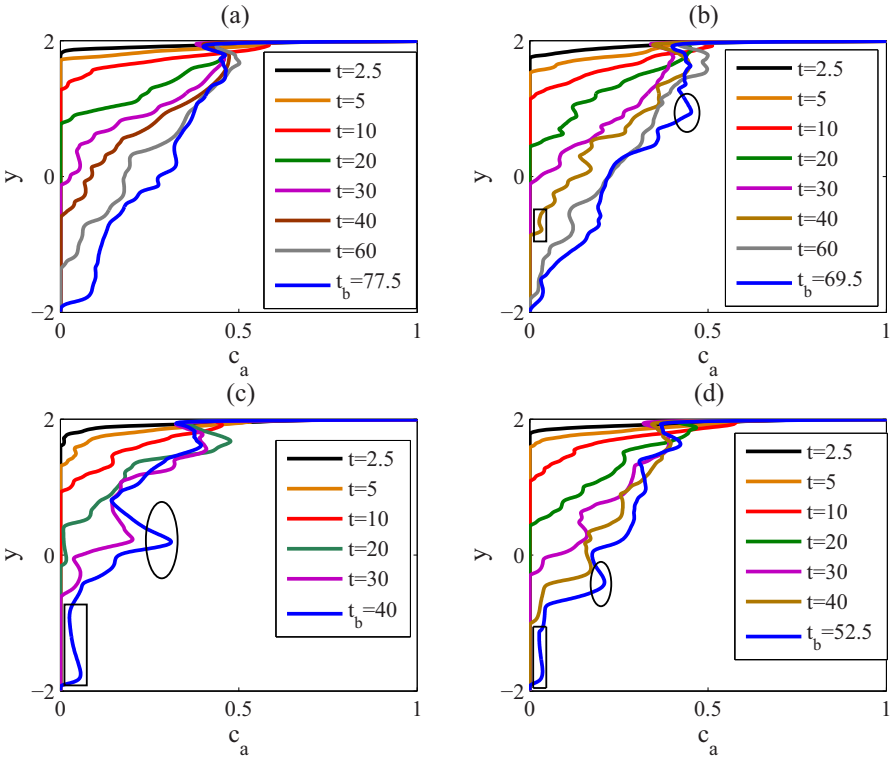

FIG. 5. Average concentration along the x axis (c_a) at different times in the R1 realizations. (a) Homogeneous condition, (b) $l = 0.08$, (c) $l = 0.8$, and (d) $l = 2$. For a homogeneous condition, the profiles are nearly linear. Two major features can be identified for cases with heterogeneity, i.e., bumps and plateaus marked by ellipses and rectangles in panels (b), (c), and (d).

are plotted in Fig. 5. All the profiles of average concentration appear as diffusive-like monotonic decreases at an early time, e.g., $t = 2.5$. This diffusive-like behavior does not persevere after a certain time, e.g., $t \geqslant 20$, 10, 10, and 20 for the homogeneous condition, $l = 0.08$, 0.8, and 2, respectively. After these times, the average profiles start to show strong influences by the permeability heterogeneity. For the conventional homogeneous case, since all the fingers evolve compatibly, the average concentration profiles of different time decease nearly linearly to the bottom boundary ($y = -2$) as shown in Fig. 5(a). If the permeability heterogeneity is present, the near linearity of average profile is no longer preserved. Two apparent features are observed leading to apparent deviations from nearly monotonic decreases as shown in Figs. 5(b)–5(d), such as local high concentration in the middle position, and nearly flat concentration profile at the bottom region. The local peak and flat region of average concentration profiles are referred to as the *bump* and *plateau* hereafter.

Formation of bumps in the concentration profile is mainly caused by the variation of a finger's width, while the plateau is formed because of the fingering competition. It can be easily observed that formation of bump and plateau is most prominent in the case of the intermediate correlation length whose breakthrough time is shortest: $l = 0.8$. To further elucidate this feature, numbers and widths of fingers, represented by the concentration profiles along the x direction, for the cases of homogeneous condition and $l = 0.8$ at several cross sections of $y = -1, -0.5, 0, 0.5$, and 1, are shown Fig. 6. For the homogeneous condition as shown in Fig. 6(a), even the number of fingers gradually decreases away from the top of domain, and widths of the fingers remain nearly unchanged. This confirms a nearly linear decrease of average concentration profile at breakthrough time as shown in Fig. 5(a). On the other hand, the widths of fingers vary greatly for the case

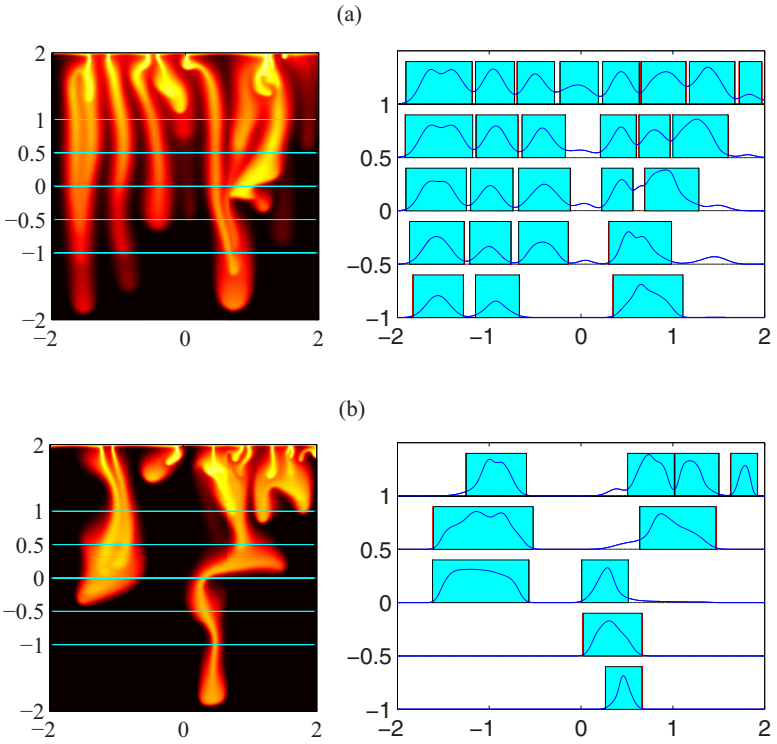

FIG. 6. Widths of fingers for five representative cross sections at $y = -1, -0.5, 0, 0.5, 1$, as shown by the lines in the left concentration images, of (a) homogeneous case and (b) $l = 0.8$. Widths of individual fingers at these cross sections are marked by blue boxes, in which the heights of these blue boxes stand for a concentration value of $c = 0.8$.

of $l = 0.8$, especially very thick fingers formed in the middle region between $0 < y < 0.5$ as shown in Fig. 6(b). This explains an apparent local bump of average concentration located at the middle region as shown in Fig. 5(c). On the other hand, the plateau is formed because of fingering competition, which is enhanced by local permeability heterogeneity as mentioned above. Very prominent fingering competition results in only a single dominant finger at $y < -0.5$ for case of $l = 0.8$, so that the local average concentration remains nearly unchanged to form a plateau on the bottom region as also shown in Fig. 5(c).

Results presented above clearly show the most significant effects of permeability heterogeneity on the fingering patterns occur in an intermediate correlation length of $l = 0.8$, which confirm the above-mentioned resonant effects. To demonstrate the prominence of fingering phenomena, vorticity and streamlines (superimposed on correspondent permeability field) for different cases, e.g., homogeneous condition, $l = 0.08$ and $l = 0.8$, at an earlier time $t = 30$ are plotted in Fig. 7. For better comparison, images of concentration are also shown. Except for the top layer of fluid 1 reservoir, the vorticity in homogeneous case, as shown in Fig. 7(b), is purely induced by viscosity contrast with local maxima at the tips of fingers. As a result, the main paths of flows, i.e., regions with denser distributions of streamlines in Fig. 7(c), are almost straight downward. If the correlation length is slightly increased to $l = 0.08$, even the number of fingers remains nearly the same as the homogeneous case, and the local maximum strengths of vorticity are increased and shifted to the middle region of fingers, where local permeability is higher, as shown Fig. 7(e). Nevertheless, the overall downward orientation of the major flow paths is not altered. If the correlation length is further raised to $l = 0.8$, local maximum vorticity is greatly enhanced at the middle region, so that fingers grow faster toward the region with high permeability.

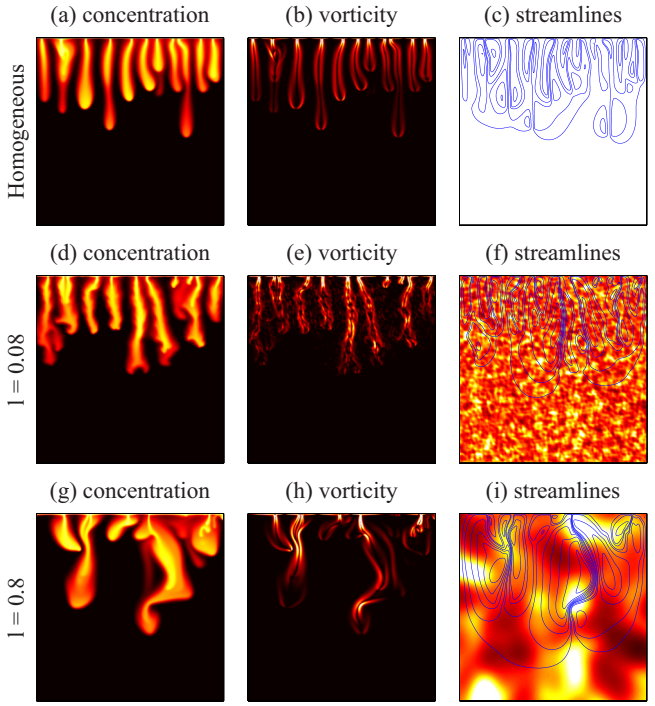

FIG. 7. Concentration (left column), vorticity (middle column), and streamlines superimposed on the correspondent permeability field (right column) at $t = 30$ in the R1 permeability realizations. Top row: homogeneous condition; middle row: $l = 0.08$; bottom row: $l = 0.8$. The brightness in the vorticity image indicates the strength of local flow activity.

To summarize this section, several qualitative features affected by heterogeneity, e.g., competition and width variation of fingers, formations of bumps and plateaus of the average concentration profiles, enhancement and position shift of local maximum vorticity, are observed and discussed. They all confirm that the strongest influence of the resonant effect occurs in an intermediate correlation length, e.g., $l = 0.8$ at the present condition. We emphasize the important issue that most of the previous studies about the influence of permeability heterogeneity on viscous fingering had been conducted in the condition associated with active displacements rather than density-driven flows. Recently the application of CO_2 storage has drawn great attention to the density-driven convection flows. The phenomena described in our present results, which show consistency with the early studies by active displacements, ensure their robustness regardless the driven sources, so they can be validly used for the CO_2 storage application. In the following section, quantitative analysis is presented to further clarify the underlined mechanism.

B. Quantitative measures: Multiple realizations of different sets of random signals

Above we discussed the influences of heterogeneity by mainly observing the fingering patterns in a representative series of permeability distribution, i.e., the R1 distribution. A question that naturally arises is the generality to other distributions associated with the same statistical parameters but generated by different sets of random signals. To verify the generality of results observed in the previous section as well as the possible variations, seven additional distributions of permeability fields are generated based on different sets of random signals, referred to as realizations R2–R8. Shown in Figs. 8 and 9 are the concentration contours superimposed on the correspondent

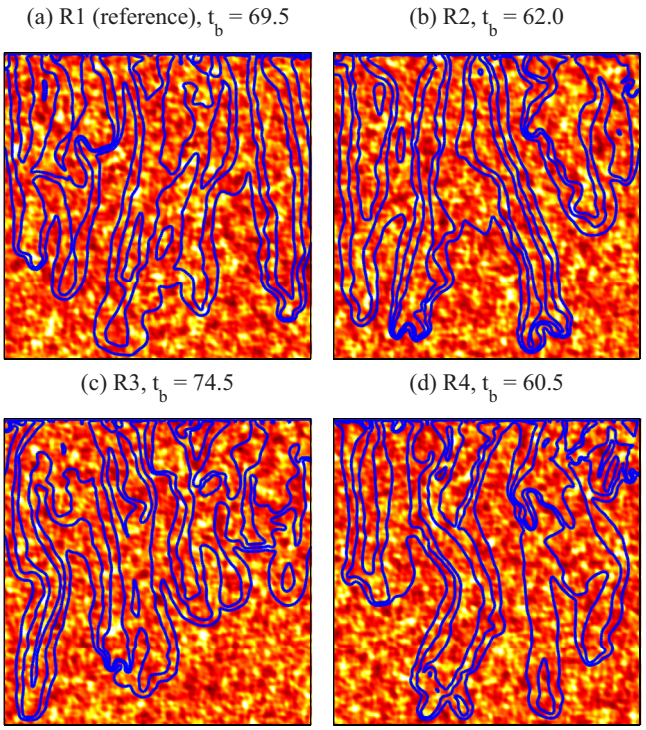

FIG. 8. Concentration contours of $c = 0.05, 0.25, 0.5$, and 0.95 superimposed on the correspondent permeability fields of $l = 0.08$ generated by various sets of random signals: (a) R1 (reference case), (b) R2, (c) R3, and (d) R4 realizations. The overall streamline patterns are similar. Fingering competition is not prominent in all the permeability distributions.

permeability fields associated with the same statistical characteristics of $l = 0.08$ and 0.8 but based on four different sets of random signals: R1 (representative realization discussed in the previous section), R2, R3, and R4. Visual qualitative observations of the fingering patterns appear consistent regardless of local random realizations of permeability for both correlation lengths. Nevertheless, while the breakthrough time varies mildly for $l = 0.08$, $t_b = 60.5$ to 74.5, great variations occur for the cases of $l = 0.8$, $t_b = 30.5$ to 59.0. These inconsistent behaviors are also observed in the profiles of average concentration as shown in Fig. 10. The four profiles of $l = 0.08$ nearly collapse on each other with the monotonic decrease. On the other hand, profiles of $l = 0.8$, where strong resonant effects are induced as stated earlier, appear very different with the apparent presence of bumps and plateaus. These indicate that important quantitative measures, at least the breakthrough time presented so far, could be affected strongly by random realizations. More thorough discussion will be given below.

As mentioned previously, the resonant effects induced in the case of $l = 0.8$ result in many interesting behaviors. The question to answer is why do the resonant effects occur in this particular correlation length? Proposed by Chen and Meiburg [24], they argued that the resonant effects occur if typical sizes of fingers are slightly less than the correlation length. To verify the argument, average widths of fingers, denoted as l_f, in all eight realizations are plotted in Fig. 11(a). The average width for every realization is calculated based on 33 cross sections between $-1 < y < 1$, in which five sample cross sections for the homogeneous case and $l = 0.8$ of the representative R1 realization are demonstrated in Fig. 6. The global mean values of fingers' widths in heterogeneous conditions are generally larger than the homogeneous condition. The mean finger's width increases for longer

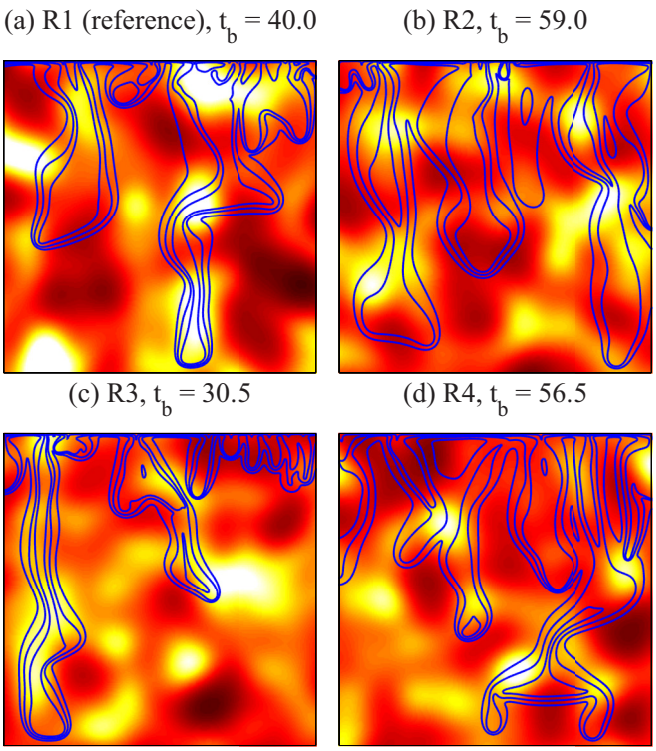

FIG. 9. Concentration contours superimposed on the correspondent permeability fields of $l = 0.8$ generated by various sets of random signals: (a) R1 (reference case), (b) R2, (c) R3, and (d) R4 realizations. Prominent fingering competition results in very distinct patterns in various distributions.

correlation length before reaching a maximum at $l = 0.8$. It is interesting to notice that the case of $l = 0.8$ is exactly the condition to induce the most significant resonant effects, in which the mean width of a finger is slightly less than the correlation length as the normalized width ($l_f/l < 1$) shown in Fig. 11(b).

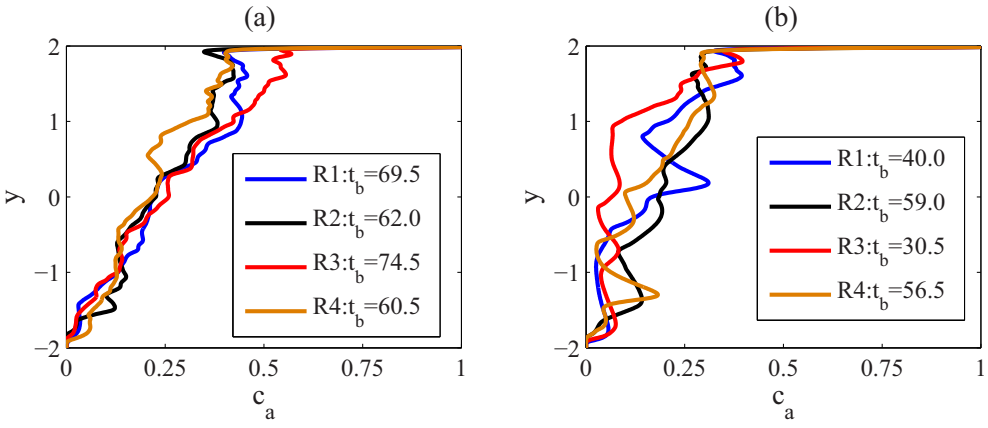

FIG. 10. Average concentration (c_a) at breakthrough time t_b in four permeability realizations: R1 (reference case), R2, R3, and R4 realizations. (a) $l = 0.08$ and (b) $l = 0.8$.

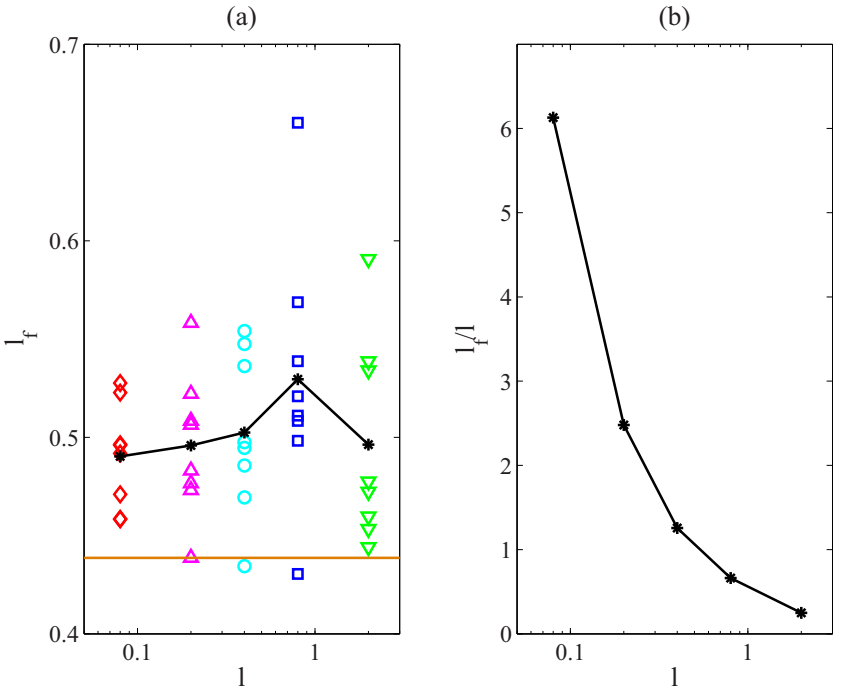

FIG. 11. (a) Mean fingers' widths (l_f) for various correlation lengths in eight permeability realizations. Mean width in a homogeneous condition is shown by the horizontal orange lines. (b) Normalized width by the corresponding correlation length (l). The normalized width decreases monotonically for larger correlation length scale.

Several quantitative measures with practical interest are also worthy of discussion. Shown in Fig. 12(a) is the breakthrough time (t_b), which indicates the arrival time of fluid transported downward. The presence of permeability heterogeneity provides additional sources of vorticity, so that the breakthrough time is generally shorter than the homogeneous condition, e.g., the global mean value of eight realizations. As mentioned previously, the shortest breakthrough time occurs in an intermediate correlation length of $l = 0.8$, whose finger's width is slightly less than the correlation length. The second measure of interest is the amount of fluid 1 downward flowing into the region originally occupied by fluid 2 at the breakthrough time, denoted as Q_b shown in Fig. 12(b). This particular measure represents the volume of CO_2-brine mixture penetrating into the ambient brine and is favorable for stable CO_2 storage. Since the total amount is closely relevant to the time allowed to flow downward, the global trend of the mean value is similar with the breakthrough times as expected. It is also noticed that these two measures can be used to approximately quantify the fingering competition described in the above section. In cases associated with less fingering competition, several fingers evolve comparably without a fast growing dominant finger, so that the breakthrough is expected to occur later. In addition, these multiple comparable fingers can accommodate more downward fluids, i.e., higher Q_b. Confirmed by Fig. 12, the strongest fingering competition occurs for an intermediate correlation length of $l = 0.8$ with earliest t_b and lowest Q_b.

Two additional measures of interests are the mixing interfacial length and the normalized mixing index at the breakthrough time, respectively denoted as L_b and σ_n^2. These two measures are highly relevant to the potential chemical reactions or pollution and shown in Figs. 12(c) and 12(d), respectively. It is also worth notice that chemical reactions are also favorable for long-term CO_2

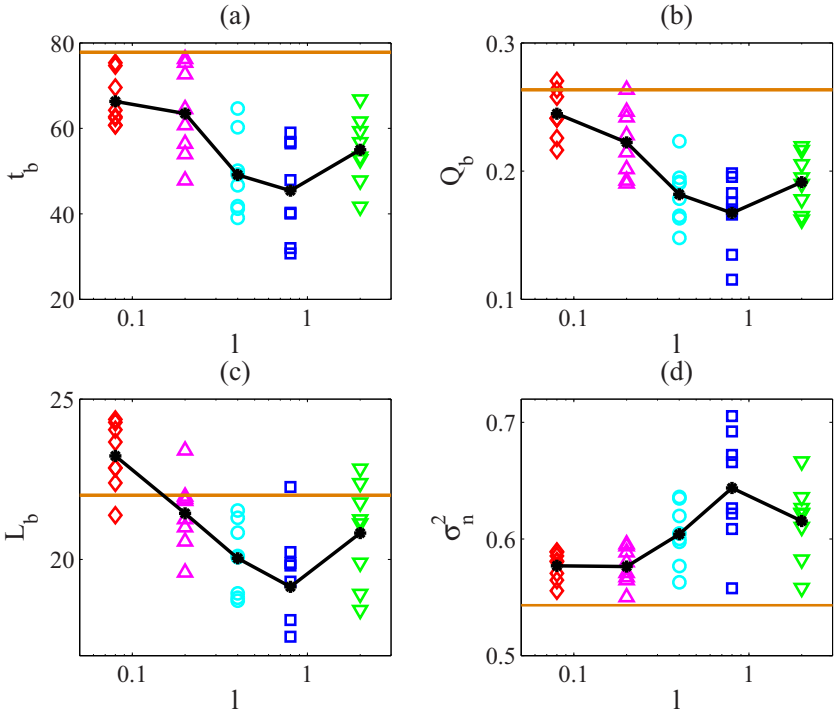

FIG. 12. Measures of interests for various correlation lengths in eight permeability realizations. (a) breakthrough time (t_b), (b) volume of lighter fluid penetrating into heavier fluid (Q_b) at $t = t_b$, (c) mixing length (L_b) at $t = t_b$, and (d) normalized mixing variance (σ_n^2) at $t = t_b$. Mean of the eight realizations is connected by the black line. Value of the corresponding measure in a homogeneous condition, which is constant, is shown by the horizontal orange line.

storage. The interfacial length in a miscible interface is approximated by

$$L = \int_x \int_y \sqrt{\left(\frac{\partial c}{\partial x}\right)^2 + \left(\frac{\partial c}{\partial y}\right)^2}\, dx\, dy. \tag{15}$$

Compared with the homogeneous condition, the mean interfacial length is longer for small correlation length of $l = 0.08$ and becomes shorter by raising the correlation length to $l = 0.4$ to reach a minimum in $l = 0.8$. The decrease of interfacial length up to $l = 0.8$ mainly results from reduction of number of fingers as well as the fingering competition. For the case of very small correlation length, whose fingers cannot fully recognize the local heterogeneity of permeability, the major fingering pattern is similar to the homogeneous condition, except a stronger dispersion to widen the finger's width. As a result, the interfacial length is generally longer than the homogeneous condition. Nevertheless, as the correlation length is raised, the channeling effects are enhanced to trigger a more prominent fingering competition. The uneven developments of fingers naturally reduce the overall interfacial length. Also, fewer fully evolved fingers in the cases of higher correlation lengths also attribute another important effect for shorter interfacial lengths.

The mixing effectiveness is determined by a normalized mixing index σ_n^2, which is obtained by

$$\sigma^2 = \frac{\sum (c - \bar{c})^2}{N^2}, \tag{16}$$

$$\sigma_n^2 = \frac{\sigma^2}{\bar{c}(1 - \bar{c})}, \tag{17}$$

where $\bar{c}$ is the mean concentration of the region originally occupied by fluid 2, and N^2 is the number of computational grids. The normalized mixing index of σ_n^2 is the indicator of mixing effectiveness compared with the similar flow in a fully immiscible condition. Higher σ_n^2 represents worse mixing effectiveness by the presence of heterogeneity. Again, the worst mixing effectiveness occurs in the case of $l = 0.8$, in which fewer fingers are fully evolved, so that the overall interfacial length is shorter to allow more molecular diffusion. In addition, the resonant effects accelerate the developments of fingers, which reduce the overall diffusive time. These two reasons explain why the worst mixing happens in the case of $l = 0.8$.

An important remark for all the above quantitative measures is their variation among different random realizations. It is interesting that the widest spreads of all these measures always occur in the resonant condition of $l = 0.8$, while the least scatterings usually happen in the smallest correlation length of $l = 0.08$. These can be understood by the competition of two major length scales: the finger's width (l_f) and the correlation length (l). In the conditions of $l \ll l_f$, the fingers may not completely recognize the local heterogeneity of permeability, so that the bulk motion of fluids is mainly dominated by the original gravitational effects. This inability to recognize the local permeability heterogeneity is the main reason why the quantitative measures in a smaller correlation length appear more closely distributed among distinct random realizations. On the other hand, for the cases when l and l_f are compatible, the regions with high permeability are wide enough to influence or even fully accommodate the fingers. It might happen in few cases if the regions of high permeability align vertically to form a connecting channel along the main flow direction (y direction), so that few dominant fingers would quickly evolve and flow downward. Another rare, but possible, scenario is the regions of lower permeability could align along the main flow path instead, so that the downward flow paths are obstructed to delay the breakthrough. Enhanced by the additional resonant effects, it is expected that the selections of flow paths in these two extreme conditions are the most sensitive to cause significant inconsistent outcomes. As a result, the local variations of all the quantitative measures among different realizations are always the largest in the resonant regime.

IV. CONCLUDING REMARKS

Effects of permeability heterogeneity in miscible porous media flows driven by gravity, which are highly relevant to the underground CO_2 storage, are studied numerically. To extend the global generality of the influences of heterogeneity, multiple permeability distributions, which are generated randomly and characterized by the two identical statistic control parameters of correlation length and variance but based on different sets of random signals, are emphasized to evaluate the global trend by mean values as well as local variations among different realizations. Two major qualitative observations of the fingering patterns, i.e., more prominent fingering competition and greater variation of fingers' widths, are found at the presence of permeability heterogeneity. These two major influences result in the earlier breakthrough time with fewer fully developed fingers in heterogeneous conditions. The resonant effects, which lead to critical behaviors, e.g., most prominent fingering competition, occur in conditions of intermediate correlation lengths. These results are consistent with the early findings in similar heterogeneous environments subjected to active injections [23–25,28,29].

Important quantitative measures of interest, including breakthrough times, volumes of lighter fluid transported, mixing lengths, and normalized mixing effectiveness, are analyzed by their statistical means based on eight random realizations. The presence of heterogeneity reduces the means of breakthrough times, fluid volume downward transported, mixing interfacial length and normalized mixing effectiveness. The resonant effect is quantitatively verified to occur in conditions in which the widths of fingers are slightly less than the correspondent correlation length and result in the most significant influence on these measures. Nevertheless, the local flow motion might be strongly affected by the predetermined distributions of applied random signals. Consequently, under the conditions associated with resonant effects, in which the flow path selection is mostly affected

by the local permeability distributions, these measures also vary the widest for a few special cases whose regions of high (or low) permeability align along with the main downward flow. The results strongly suggest cautious implementations in the resonant regime to consider these local variations, but merely relying on the global means, even the statistical parameters are identical.

ACKNOWLEDGMENTS

Support by the Ministry of Science and Technology, Taiwan (MOST 105-2221-E-009-074-MY3) and the National Natural Science Foundation of China (Grants No. 51421063 and 51576051) is acknowledged.

[1] P. G. Saffman and G. I. Taylor, The penetration of a fluid into a porous medium or Hele-Shaw cell containing a more viscous liquid, Proc. R. Soc. London Ser. A **245**, 312 (1958).
[2] G. M. Homsy, Viscous fingering in porous media, Annu. Rev. Fluid Mech. **19**, 271 (1987).
[3] K. V. McCloud and J. V. Maher, Experimental perturbations to Saffman-Taylor flow, Phys. Rep. **260**, 139 (1995).
[4] F. M. Orr, Onshore geologic storage of CO_2, Science **325**, 1656 (2009).
[5] S. M. V. Gilfillan, B. S. Lollar, G. Holland, D. Blagburn, S. Stevens, M. Schoell, M. Cassidy, Z. Ding, Z. Zhou, G. Lacrampe-Couloume, and C. J. Ballentine, Solubility trapping in formation water as dominant CO_2 sink in natural gas fields, Nature (London) **458**, 614 (2009).
[6] H. E. Huppert and J. A. Neufeld, The fluid mechanics of carbon dioxide sequestration, Annu. Rev. Fluid Mech. **46**, 255 (2014).
[7] J. M. Matter, M. Stute, S. Snæbjornsdottir, E. H. Oelkers, S. R. Gislason, E. S. Aradottir, B. Sigfusson, I. Gunnarsson, H. Sigurdardottir, E. Gunnlaugsson, G. Axelsson, H. A. Alfredsson, D. Wolff-Boenisch, K. Mesfin, D. F. de la Reguera Taya, J. Hall, K. Dideriksen, and W. S. Broecker, Rapid carbon mineralization for permanent disposal of anthropogenic carbon dioxide emissions, Science **352**, 1312 (2016).
[8] E. Lindeberg and D. Wessel-Berg, Vertical convection in an aquifer column under a gas cap of CO_2, Energy Convers. Manage. **38**, S229 (1997).
[9] F. Nadal, P. Meunier, B. Pouligny, and E. Laurichesse, Stationary plume induced by carbon dioxide dissolution, J. Fluid Mech. **719**, 203 (2013).
[10] A. Vreme, F. Nada, B. Pouligny, P. Jeandet, G. Liger-Belair, and P. Meunier, Gravitational instability due to the dissolution of carbon dioxide in a Hele-Shaw cell, Phys. Rev. Fluids **1**, 064301 (2016).
[11] S. Backhaus, K. Turitsyn, and R. E. Ecke, Convective Instability and Mass Transport of Diffusion Layers in a Hele-Shaw Geometry, Phys. Rev. Lett. **106**, 104501 (2011).
[12] P. A. Tsai, K. Riesing, and H. A. Stone, Density-driven convection enhanced by an inclined boundary: Implications for geological CO_2 storage, Phys. Rev. E **87**, 011003 (2013).
[13] A. C. Slim, M. M. Bandi, J. C. Miller, and L. Mahadevan, Dissolution-driven convection in a Hele-Shaw cell, Phys. Fluids **25**, 024101 (2013).
[14] J. H. Ching, P. Chen, and P. A. Tsai, Convective mixing in homogeneous porous media flow, Phys. Rev. Fluids **2**, 014102 (2017).
[15] A. Riaz, M. Hesse, H. A. Tchelepi, and F. M. Orr, Onset of convection in a gravitationally unstable diffusive boundary layer in porous media, J. Fluid Mech. **548**, 87 (2006).
[16] K. Ghesmat, H. Hassanzadeh, and J. Abedi, The impact of geochemistry on convective mixing in a gravitationally unstable diffusive boundary layer in porous media: CO_2 storage in saline aquifers, J. Fluid Mech. **673**, 480 (2011).
[17] M. L. Szulczewski, M. A. Hesse, and R. Juanes, Carbon dioxide dissolution in structural and stratigraphic traps, J. Fluid Mech. **736**, 287 (2013).
[18] X. Fu, L. Cueto-Felgueroso, D. Bolster, and R. Juanes, Rock dissolution patterns and geochemical shutdown of CO_2-brine-carbonate reactions during convective mixing in porous media, J. Fluid Mech. **764**, 296 (2015).

[19] M. De Paoli, F. Zonta, and A. Soldati, Influence of anisotropic permeability on convection in porous media: Implications for geological CO_2 sequestration, Phys. Fluids **28**, 056601 (2006).
[20] M. De Paoli, F. Zonta, and A. Soldati, Dissolution in anisotropic porous media: Modelling convection regimes from onset to shutdown, Phys. Fluids **29**, 026601 (2017).
[21] M. Bestehorn and A. Firoozabadi, Effect of fluctuations on the onset of density-driven convection in porous media, Phys. Fluids **24**, 114102 (2012).
[22] R. Blackwell, J. Rayne, and W. Terry, Factors influencing the efficiency of miscible displacement, Petrol. Trans. AIME **217**, 1 (1959).
[23] C. T. Tan and G. M. Homsy, Viscous fingering with permeability heterogeneity, Phys. Fluids A **4**, 1099 (1992).
[24] C.-Y. Chen and E. Meiburg, Miscible porous media flows in the quarter five-spot configuration. Part 2: Effect of heterogeneities, J. Fluid Mech. **371**, 269 (1998).
[25] E. Meiburg and C.-Y. Chen, High-accuracy implicit finite-difference simulations of homogeneous and heterogeneous miscible porous medium flows, SPE J. **5**, 129 (2000).
[26] E. Camhi, E. Meiburg, and M. Ruith, Miscible rectilinear displacements with gravity override. Part 2. Heterogeneous porous media, J. Fluid Mech. **420**, 259 (2000).
[27] C.-Y. Chen and E. Meiburg, Miscible porous media flows in the quarter five-spot configuration. Part 1: The homogeneous case, J. Fluid Mech. **371**, 233 (1998).
[28] C.-Y. Chen and P.-Y. Yan, A diffuse interface approach to injection-driven flows of different miscibility in heterogeneous porous media, Phys. Fluids **27**, 083101 (2015).
[29] C.-Y. Chen and P.-Y. Yan, Radial flows in heterogeneous porous media with a linear injection scheme, Comput. Fluids **142**, 30 (2017).
[30] C.-Y. Chen, T.-S. Lin, and J. A. Miranda, Rotationally induced fingering patterns in a two-dimensional heterogeneous porous medium, Phys. Rev E **94**, 053105 (2016).
[31] J.-S. Li, Q. Li, W. Cai, F.-C. Li, and C.-Y. Chen, Mixing efficiency via alternating injection in a heterogeneous porous medium, J. Mech. **34**, 167 (2018).
[32] U. G. Araktingi and F. M. Orr, Jr., Viscous fingering in heterogeneous porous media, SPE Adv. Tech. Ser. **1**, 71 (1993).
[33] A. DeWit and G. M. Homsy, Viscous fingering in periodically heterogeneous porous media. 1. Formulation and linear instability, J. Chem. Phys. **107**, 9609 (1997).
[34] A. Riaz and E. Meiburg, Vorticity interaction mechanisms in variable-viscosity heterogeneous miscible displacements with and without density contrast, J. Fluid Mech. **517**, 1 (2004).
[35] M. Sajjadi and J. Azaiez, Scaling and unified characterization of flow instabilities in layered heterogeneous porous media, Phys. Rev. E **88**, 033017 (2013).
[36] M. Shinozuka and C.-M. Jan, Digital simulation of random processes and its applications, J. Sound Vib. **25**, 111 (1972).
[37] Y.-S. Huang and C.-Y. Chen, A numerical study on radial Hele-Shaw flow: Influence of fluid miscibility and injection scheme, Comput. Mech. **55**, 407 (2015).